Journal of Alloys and Compounds 672 (2016) 510–520

Contents lists available at ScienceDirect

Journal of Alloys and Compounds

journal homepage: http://www.elsevier.com/locate/jalcom

First principles exploration of near-equiatomic NiFeCrCo high entropy alloys

C. Niu, A.J. Zaddach, C.C. Koch, D.L. Irving*

Department of Materials Science and Engineering, North Carolina State University, Raleigh, NC 27695 USA

ARTICLE INFO

Article history:
Received 7 November 2015
Received in revised form
25 January 2016
Accepted 12 February 2016
Available online 16 February 2016

Keywords:
High entropy alloy
Elastic properties
Density functional theory

ABSTRACT

High entropy alloy NiFeCrCo was systematically studied in the range of near-equal atomic concentrations, i.e., 10–40 at.%, by first-principles tools and high throughput calculations. Enthalpy of mixing, lattice parameter (a_0), bulk modulus (B), and shear modulus (G) were calculated by the exact muffin-tin orbital method combined with coherent potential approximation (EMTO-CPA) for over 2700 compositions of the NiFeCrCo alloy as a single-phase solid solution in paramagnetic state. It was found that certain elements have the most significant influence on each property, namely, Cr on enthalpy of mixing, Co on a_0, Fe on B, Co on G, and Cr on the ratio of B/G. An equation to predict the enthalpy of mixing by use of binary enthalpy data was evaluated and was found to have a good accuracy with a root-mean-square deviation (RMSD) of 42 meV per formula unit in the prediction. A similar equation to predict bulk modulus with weighted contribution from first–shell interaction is proposed and tested on all alloys. This equation was also found to be accurate with a RMSD of 6 GPa. Finally, it was found that shear moduli of all tested alloys are largely dependent on C_{44}, while the concentration of Co has a noticeable control on C_{44}. Spin polarized calculations were performed for a select group of alloys with both EMTO-CPA and the Vienna *ab-initio* Simulation Package (VASP) with special quasi-random structure models for comparison. Good agreement was found between these methods.

1. Introduction

There has been a rapid growth in interest in multi-component equiatomic metallic alloys that form as random solid solutions on simple lattices since their independent discoveries by the groups of Yeh [1] and Cantor [2]. These alloys consist of at least four elements with each elemental compositions between 5 and 35 at.%. This class of alloy was labeled a high entropy alloy (HEA) due to the higher configurational entropy present in the multi-component equiatomic system. HEAs have also motivated the study of other non-traditional alloys referred to as compositionally complex alloys [3]. These alloys deviate from conventional alloying strategies (i.e. a primary solvent with solutes in low concentrations) but do not quite fit the definition of HEAs.

HEAs are of significant interest because of their desirable combinations of physical properties. To name a few examples, yield strength up to about 3000 MPa has been reported in the bcc $AlNiFeCrCoTi_x$ system [4]. Refractory VNbMoTaW has a high strength at elevated temperatures up to 1800 K [5]. $Al_{0.5}$ NiFeCrCoCu HEAs has great fatigue resistance [6]. And NiFeCrCoTi and AlNiFeCrCoTi HEAs have great wear resistance [7]. However, issues of alloy phase stability, fundamental mechanisms responsible for physical properties, and the development of predictive rules that facilitate the selection of new alloy compositions are areas that are still being developed.

Previous to the discovery of HEAs, it was believed that multi-component alloys would favor the formation of structurally amorphous bulk metallic glasses (BMGs) or would lead to multi-phase intermetallic alloys. Unlike these systems, HEAs form solid solutions on simple lattices (e.g., fcc, bcc, and hcp). This has been attributed to the fact that HEAs tend to have an enthalpy of mixing close to zero, making them an ideal solution and enabling entropy to dominate the free energy [8]. Also important in HEA formation are the relative atomic sizes and atomic species making up the alloy. Generally, an HEA forms when constituent elements possess similar metallic radii [8].

The relative atomic size constraint in forming an HEA has led to research into alloy groups that can be classified by the average metallic radius of constituent elements. For the purpose of grouping

* Corresponding author.
E-mail address: dlirving@ncsu.edu (D.L. Irving).

http://dx.doi.org/10.1016/j.jallcom.2016.02.108
0925-8388/

HEAs, Al serves as a convenient (yet arbitrary) reference element with a metallic radius of 0.143 nm. HEAs formed of elements with a metallic radius greater than Al have been pursued for high temperature [5] or low density [9] applications. Elements with a radius smaller than Al are generally transition metals and can be grouped into 3*d*, 4*d*, or 5*d* sub-groups. Many of the 4*d* and 5*d* transition metals have a similar metallic radii between 0.135 and 0.140 nm and a group of 3*d* elements (Cr, Mn, Fe, Co, Ni, and Cu) have metallic radii between 0.125 and 0.128 nm. Due to the many practical structural applications, their desirable combination of properties for these applications, and the ability to form single phase random solid solutions, combinations containing Co, Cr, Fe, Mn, and Ni have been some of the most widely studied HEAs.

Equiatomic NiFeCrCoMn was one of the earliest HEAs identified [2]. It and its equiatomic base alloy, NiFeCrCo, have been of interest to the tuning of properties and phase stability in Ref. 3*d* HEAs. Recent interest has focused on both developing a fundamental understanding of the properties and stability of these equiatomic HEAs as well as optimization of properties of the HEA for engineering purposes. Examples include investigation of the phase stability [10–13], local chemical ordering [14–16], mechanical [17–25], and magnetic [14,16,26–28] properties. Equiatomic NiFeCrCo was found to remain a coherent fcc crystal lattice as milled [24] or after annealing for a week [29], and have good strength and excellent ductility [20,24]. Recent results that combined density functional theory and experimental techniques, including magnetization measurement and scanning transmission electron microscopy, identified nanodomains where Cr orders in an $L1_2$ structure [14]. Later Monte Carlo calculations using first principles methods supported the conclusion that Cr should order and is magnetically frustrated in the disordered random solid solution phase [16]. Equiatomic NiFeCrCoMn also forms as a fcc solid solution phase as milled or cast [24]. This equiatomic quinary HEA was found to also have a balanced performance in strength and ductility [18,20,24], and have remarkable fracture resistance at cryogenic temperatures [19].

Given that a good combination of strength and ductility is possessed by equiatomic NiFeCrCo and NiFeCrCoMn, investigation of near-equiatomic compositions is of interest in that better performance may be realized in this range. However, systematic study of the non-equiatomic compositions of either NiFeCrCo or NiFeCrCoMn HEAs is a significant challenge due to the vast number of possible alloy combinations. Furthermore, experimental investigations are hindered by the lack of validated predictive theories for mechanical properties and the huge number of samples to manufacture for such studies. Computational tools, on the other hand, provide an efficient and economic path towards a systematic prediction of the relation between near-equiatomic HEA compositions and properties.

In the present work, we report our computational exploration of the near-equiatomic range of the four-component NiFeCrCo HEAs in the random solid solution phase. We have explored the near-equiatomic range of Ni–Fe–Cr–Co high entropy alloys in terms of enthalpy of mixing, lattice parameters, bulk moduli, elastic constants, shear moduli, and B/G ratio. Detailed maps of these properties are obtained. Additionally we evaluate the validity of equations that allow convenient estimate of enthalpy of mixing as well as bulk modulus using only properties of binary alloys. These equations are found to capture general trends in alloying and are sufficient for qualitative estimates of the physical property of interest. For each element, the element that dominates the macroscopic behavior is identified. Ultimately, this data may be used by those interested in tuning the physical properties of interest.

With that said, this work focuses on the prediction of the properties of random solid solutions of these non-equiatomic HEAs. It is outside the scope of the present work to evaluate whether each 2700 + compositions of the alloys evaluated remain single phase solid solutions over the entirety of the composition range. There are a limited number of reports that suggest that this is not always the case for particular elements. For example, as Cr is enriched, there is evidence of σ phase formation together with the random solid solution [30]. Additionally, local ordering of elements is not explored as was seen in nano domains of annealed NiFeCrCo [14]. In both situations, the random solid solution matrix is present and its properties may contribute to a significant fraction of the macroscopic response. As such, the predictions presented in this manuscript are still a valuable aid in interpreting the physical properties of these more complex alloys whose properties depend on the collective interaction of the random solid solution with the secondary phases. Furthermore, non-equilibrium synthesis methods routinely produce solid solutions and due to the slow diffusion [11] these alloys are metastable for extended periods. Throughout the discussion, we note when results are discussed in regions known to diverge from known single phase random solid stability.

2. Computational methods

Two complementary first principles methods were used in the present study. The first was the Exact Muffin-Tin Orbital method combined with Coherent Potential Approximation (EMTO-CPA). Overlapping muffin-tin potential spheres were used to accurately describe the exact one-electron potential. The EMTO method calculates total energy using the full charge density (FCD) technique [31]. FCD calculations have similar accuracy to that of full-potential methods but are more computationally efficient. The CPA technique allows simulation of random solid solutions by blending constituent potentials into one single site [32]. The nature of this one-site approximation by CPA ignores local lattice displacement. In spite of this, the EMTO-CPA method has been shown to be accurate for HEA systems composed of transition metals [14,24,25,33,34]. The second method was the Vienna *Ab-initio* Simulation Package (VASP) [35,36] with projector augmented wave (PAW) pseudopotentials [37,38]. Special quasi-random structures (SQS) [39], which are atomic models that best represent the targeted alloy within the confines of the periodic boundary condition, were generated through a Monte Carlo algorithm [40]. For both calculation methods, the Perdew-Burke-Ernzerhof version of generalized gradient approximation (GGA-PBE) of exchange-correlation functionals was used [41,42].

For the EMTO calculations, the Kohn–Sham equations were solved within the soft-core approximation in which the core states are recalculated after each iteration. This was recently shown to give elastic constants close to those measured experimentally for equiatomic HEAs [25]. The Green's function was calculated for 16 complex energy points. The basis set of EMTO included *s*, *p*, *d*, and *f* states. A 13 × 13 × 13 k-point mesh was used; the total energy converged within 1 meV/atom. The Screened Impurity Model (SIM) parameter of 0.902 was applied for electrostatic correction to the single-site CPA. It's worth noting that this SIM parameter was found to have negligible electrostatic error for NiFeCrCo alloys [25]. We used the disordered local moment (DLM) approach to describe the paramagnetic state of Ni–Fe–Cr–Co HEAs [43]. Within the DLM model, each magnetic element was regarded as two separate parts with up and down spins. In this case, all HEAs were simulated as Fe↑ Fe↓ NiCrCo.

In the VASP calculations of pure metals, all k-point mesh settings were tested to meet the 1 meV/atom convergence criterion. We implemented a 17 × 17 × 17 for fcc Ni, bcc Fe, and bcc Cr, and 21 × 21 × 13 for hcp Co. VASP was also used to calculate the lattice parameter, bulk moduli, and shear moduli of six selected non-

equiatomic alloys. The super cells used to simulate the alloys were based on three SQS models, where the identity of the atom on each site was interchanged to simulate alloys of different compositions. The three SQS models were initiated from a conventional 4-atom fcc cell. Cells with nearly equal and long super cell lengths were prioritized. Ultimately, the super cell vectors of the SQS cell for an alloy of composition $A_{10}B_{10}C_{40}D_{40}$ were (4 −1 0), (4 0 1), and (−1 −3 3), where *A*~*D* are four placeholders for the actual chemical elements. The super cell vectors for the SQS simulating the $A_{10}B_{16}C_{34}D_{40}$ were (−1 2 −3), (−1 −3 2), and (−1 2 2), and those of the super cell simulating the $A_{10}B_{24}C_{34}D_{40}$ alloy were (−2 −2 1), (−2 −1 2), and (−1 3 −1). A k-point mesh of 3 × 3 × 3 was applied for all 100-atom SQS models. For all VASP calculations, the plane-wave cut-off energy was taken as 350 eV. The reciprocal space energy integration was performed by the Methfessel-Paxton technique [44]. SQS structures were run with and without atomic relaxations to compare with results from the EMTO method. All VASP calculations were spin polarized.

In both the EMTO-CPA and VASP calculations, equilibrium lattice parameters and bulk modulus were obtained by fitting volume-energy data to the Vinet equation of state (EOS) [45]. Compared to the Birch-Murnaghan EOS, our tests indicate that the Vinet EOS was more insensitive to the volume range when determining the bulk modulus for Ni–Fe–Cr–Co HEAs. Volumetric deformation in the range of ~±9% (i.e., lattice parameter varying ~±3%) was applied to the unit cell for Vinet EOS calculations. A cubic lattice has three independent lattice constants: C_{11}, C_{12}, and C_{44}. The calculation of these elastic constants used a method suggested by Mehl *et al.* [46] and has been implemented previously for HEAs [33]. C_{11} and C_{12} were derived from the bulk modulus B_0 and the tetragonal shear modulus C', given that $B = (C_{11} + 2C_{12})/3$ and $C' = (C_{11} - C_{12})/2$. The calculation of C' and C_{44} was based on a volume-conserving orthorhombic deformation ε_0 and monoclinic deformation ε_m, respectively, which are given by:

$$\varepsilon_0 = \begin{pmatrix} 1+\delta & 0 & 0 \\ 0 & 1-\delta & 0 \\ 0 & 0 & \dfrac{1}{1-\delta^2} \end{pmatrix} \text{ and } \varepsilon_m = \begin{pmatrix} 1 & \delta & 0 \\ \delta & 1 & 0 \\ 0 & 0 & \dfrac{1}{1-\delta^2} \end{pmatrix} \quad (1)$$

where δ was between 0.00 and 0.05 in increments of 0.01. The values of C' and C_{44} were determined by fitting the energy-deformation data to $E = E_0 + 2VC'\delta^2$ and $E = E_0 + 2VC_{44}\delta^2$, respectively.

Polycrystalline shear modulus was derived via the Voigt-Reuss-Hill averaging method [47], which defines the shear modulus G as an average of the lower (G_R) and upper (G_V) bounds given by:

$$G_R = \frac{5(C_{11} - C_{12})C_{44}}{4C_{44} + 3(C_{11} - C_{12})} \quad \text{and} \quad G_V = \frac{C_{11} - C_{12} + 3C_{44}}{5} \quad (2)$$

3. Results and discussion

While binary alloys require a 2-D diagram to cover alloying compositions and ternary alloys need a 2-D contour plot, compositions of a quaternary alloy form a 3-D contour space. A large number of configurations, therefore, need to be explored when

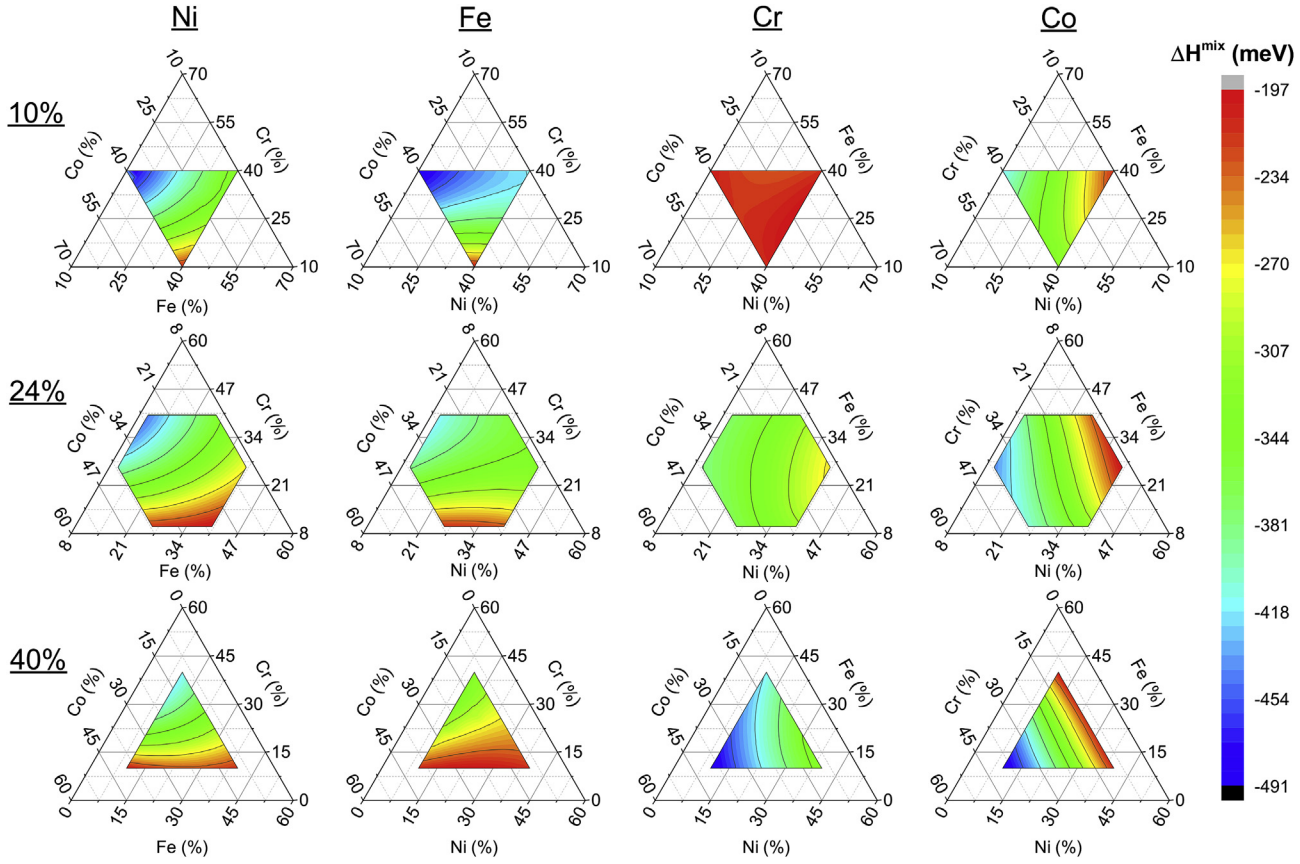

Fig. 1. Enthalpy of mixing, ΔH^{mix}, as a function of composition in Ni–Fe–Cr–Co HEAs. Each sub-plot represents a cross section in the 3-D compositional tetrahedron with one component fixed at a concentration, all other components ranging from 10 to 40 at.%.

Table 1
Lattice parameters and bulk moduli of Ni, Fe, Cr, and Co from SP EMTO calculations. For Co (hcp), the lattice parameter is reported as a/c.

		a_0 (Å)			B_0 (GPa)		
	Lat.	EMTO	VASP	Expt. [50].	EMTO	VASP	Expt. [50].
Ni	fcc	3.53	3.52	3.52	199	198	186
Fe	bcc	2.84	2.83	2.87	185	186	168
Cr	bcc	2.85	2.87	2.88	256	178	190
Co	hcp	2.50/4.04	2.49/4.02	2.51/4.07	212	211	191

evaluating the physical properties of non-equiatomic quaternary HEAs as a function of composition. We evaluate the physical properties of these alloys within the constraints that each element is allowed to vary between 10 at.% to 40 at.% in steps of 2 at.%. This creates a total of 2736 compositions explicitly calculated. For each composition multiple calculations were required to fit relevant equations of state discussed previously. To accomplish this, the majority of the results were determined by use of the EMTO + CPA method. VASP + SQS calculations were used to validate these calculations on a smaller subset of systems that we found to have interesting physical properties. Finally, in the following discussions, all concentrations are atomic percentages.

The large number of configurations calculated also presents a practical challenge of how to best present the data in a way to highlight trends present. To this end, we first present contour maps of selected slices through compositional space for the properties studied in this paper. Although data included in the contour maps represent only a portion of all data calculated, we find these maps facilitate the illustration of trends in physical property as a function of composition. The slices are organized collectively as follows. For presentation, we select an element (*column*) and fix its concentration to 10 at.%, 24 at.%, and 40 at.% (*rows*). Each of the other non-fixed elements is varied and the physical properties are presented in each individual contour map. All contour plots for each slice of the same property have the same color scale for the sake of absolute comparison between one contour plot and the next. More detailed analysis beyond these contour maps that includes evaluation of all points follows this presentation.

3.1. Enthalpy of mixing

Enthalpy of mixing originated from the calculation of the heat of mixing of a liquid in forming a solution [48]. It has also been used to predict the likelihood of random solid solution phases in metallic alloys. Recently, this has been extended to high entropy alloys, where predictions are often based on extrapolating from known binary enthalpy of mixing data [8]. For random alloys in solid state, in a similar way to liquids, enthalpy of mixing can be defined as the energy required to mix constituent atoms on the same crystal lattice. Taking the fcc NiFeCrCo alloy as an example, its enthalpy of mixing is the energy difference between the fcc alloy and constituent elements in fcc lattice, as given in Eq. (3):

$$\Delta H^{\mathrm{mix}} = E_0 - \sum c_i E_i^{\mathrm{fcc}} \tag{3}$$

where E_i^{fcc} is the ground state energy of each element i in the same fcc lattice as the alloy. Meanwhile, enthalpy of formation is defined by Eq. (4):

$$\Delta H^{\mathrm{f}} = E_0 - \sum c_i E_i^{\mathrm{stable}} \tag{4}$$

where E_i^{stable} is the ground state energy of each element i in its stable phase at 0 K. The enthalpy of formation is used to determine how favorable it is to form a particular phase as compared to the pure stable phases. At finite temperature, entropic contributions need to be considered and free energies need to be evaluated. The enthalpies of mixing and formation are related through Eq. (5), which accounts for the differences in energies of the elemental references (i.e. fcc vs. stable phases).

$$\Delta H^{\mathrm{f}} = \Delta H^{\mathrm{mix}} + \sum c_i \left(E_i^{\mathrm{fcc}} - E_i^{\mathrm{stable}} \right) \tag{5}$$

In the present work we explicitly determine the enthalpy of mixing of the multi-component alloys and compare these to data derived from extrapolation from binary enthalpy of mixing data, as the later has been widely used in the literature to predict whether alloys form as HEAs [8]. We conclude that for the alloy studied here there is a reasonable agreement between these two approaches and attempt to quantify the associated error. All enthalpy of mixing in the present work are expressed as energy per formula unit.

Twelve contour map slices in the 3-D compositional space are plotted in Fig. 1. As noted previously, each *column* has a constrained concentration of the element listed on top while the other three elements form a ternary contour. Each *row* of the array changes the composition of the constrained element.

From the data, it can be seen that Cr has the most significant influence on the enthalpy of mixing. Low concentrations of Cr lead to a higher ΔH^{mix} while higher concentrations lead to lower, more negative, ΔH^{mix}. This is most pronounced when inspecting the Cr column of Fig. 1. In this column the least negative values are when Cr is constrained at a concentration of 10 at.% and most negative when Cr is present in a concentration of 40 at.%. This trend is also visible in the contour maps for all other elements. In these contours, the enthalpy of mixing moves to its highest value (red) as the Cr concentration is reduced and its lowest value (blue) when Cr concentration is increased, with the enthalpy of mixing being most negative for the composition of Ni_{10} Fe_{10} Cr_{40} Co_{40}.

Table 2
Enthalpy of mixing (meV per formula unit) of fcc binary alloys from EMTO-CPA.

NiFe	NiCr	NiCo	FeCr	FeCo	CrCo
−93	−223	65	−149	−49	−291

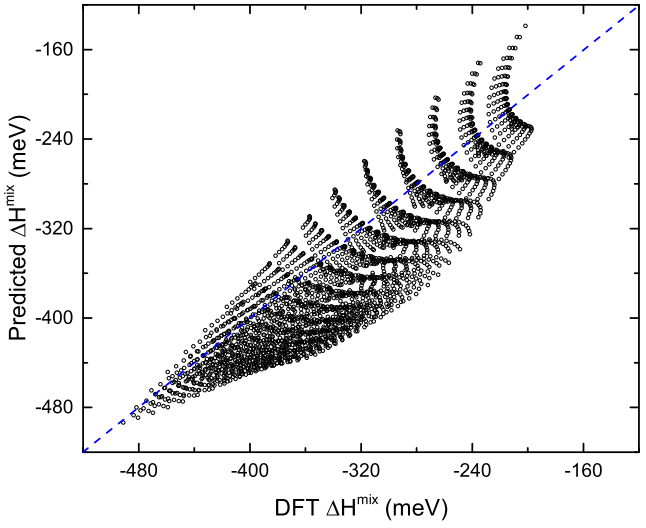

Fig. 2. Enthalpy of mixing from DFT calculations vs. predicted values from binary data for 2736 compositions of NiFeCrCo. The two enthalpies are the same on the blue dashed line, where the prediction is 100% accurate (For interpretation of the references to color in this figure legend, the reader is referred to the web version of this article.).

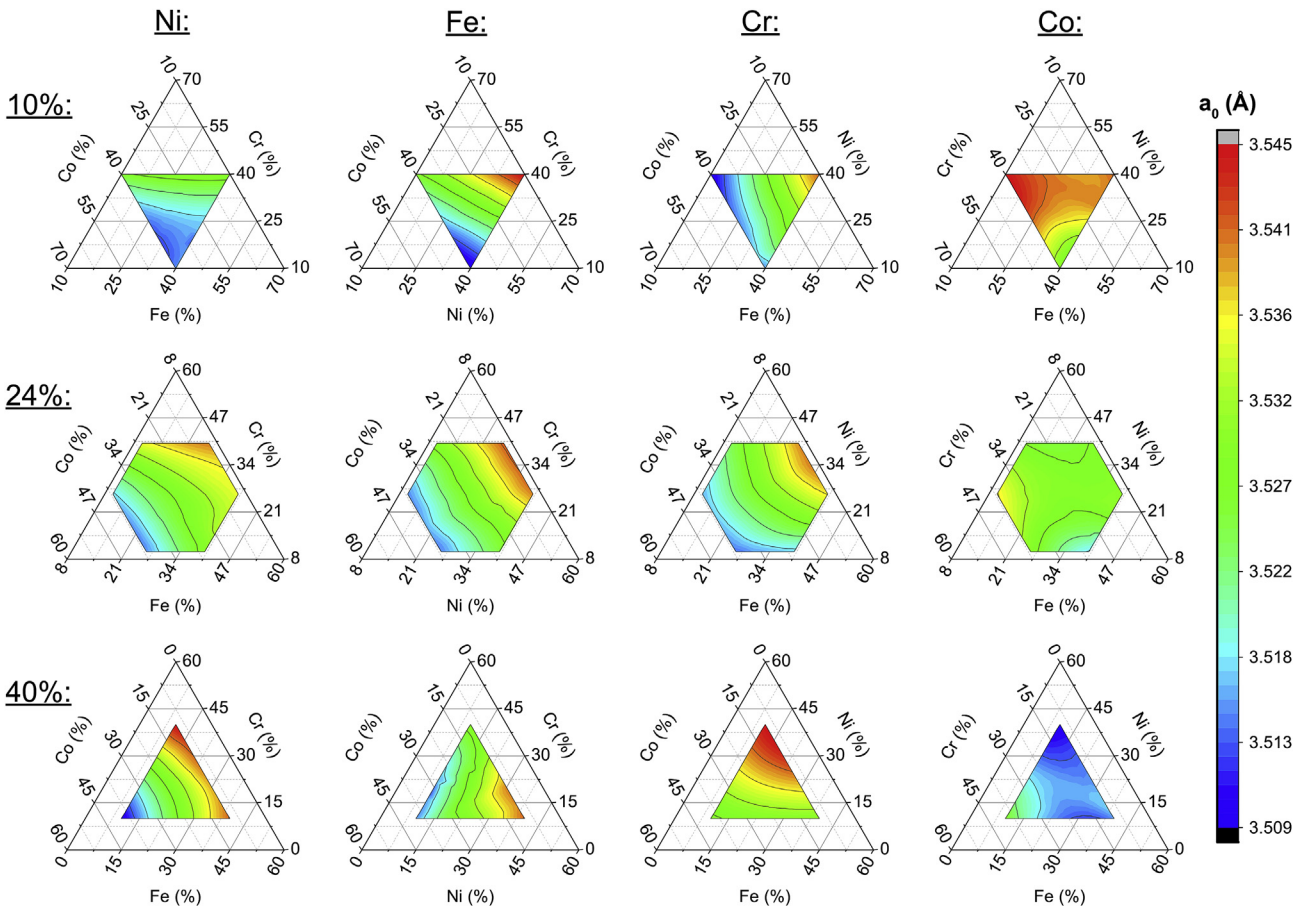

Fig. 3. Lattice parameter, a_0, as a function of composition in Ni–Fe–Cr–Co HEAs.

Enthalpy of mixing plays an important role in predicting whether a solid solution phase is energetically preferred [8]. Only enthalpy of mixing with magnitude close to zero favors the solid solution phase. Strongly negative enthalpy of mixing is inclined to lead to intermetallic compound and strongly positive enthalpy of mixing may cause separation or segregation of elements [8]. Low Cr HEAs have enthalpy of mixing closest to zero, and therefore are most likely to form solid solution phases. High concentrations of Cr/Co and low concentrations of Ni/Fe together lead to the most negative enthalpy of mixing, suggesting the possibility of formation of secondary intermetallic phases. This conclusion is consistent with recent experimental results that identified the intermetallic σ phase formation in HEAs with high concentrations of Cr ($NiFeCr_2Co$) along with an fcc random solid solution after aging the alloy at 700° C [30]. The composition of the alloy synthesized experimentally lies in the center of the 40% Cr map in Fig. 1 and has a enthalpy of mixing of −400 meV.

3.1.1. Analysis of multi-component enthalpy of mixing

As opposed to direct calculation of the enthalpy of mixing of multi-component metallic glasses, it has been proposed that this can be determined by a compositionally weighted sum consisting of mixing enthalpy of constituent *binary* alloys via [49].

$$\Delta H^{\text{mix}} = \sum_{i=1, i>j}^{n} 4 c_i c_j \Delta H_{ij}^{\text{mix}} \tag{6}$$

Eq. (6) has been used to approximate the enthalpy of mixing for multi-component solid solution high entropy alloys [8]. Here we look to use Eq. (6) to not only understand trends in the enthalpy of mixing data but also look to use the large number of data points calculated here to evaluate whether this expression qualitatively or quantitatively captures trends.

Table 3
Top 3 alloys with highest/lowest lattice parameter.

Ni,Fe,Cr,Co%	a_0 (Å)	Ni,Fe,Cr,Co%	a_0 (Å)
40, 10, 10, 40	3.509	38, 12, 40, 10	3.545
38, 10, 12, 40	3.510	40, 10, 40, 10	3.545
38, 12, 10, 40	3.510	36, 14, 40, 10	3.545

3.1.2. Data of pure metals and binary alloys

Before we begin the evaluation of the binary enthalpy of mixing equation, we first look to validate our methods against known experimental data. To do this, we first calculated the bulk properties of the constituent elements, Ni, Fe, Cr, and Co, using both the EMTO method and VASP *in their stable phases*. No restrictions were applied to these spin polarized calculations such that the structures as well as magnetic moments were fully relaxed to reach the lowest energy. Lattice parameters and bulk moduli of these metals in their naturally stable phases were calculated, namely, Ni in fcc, Fe in bcc, Cr in bcc, and Co in hcp. The calculated results were then compared with experimental measurements from the literature [50] in Table 1.

As shown in Table 1, EMTO and VASP calculations produce lattice parameters and bulk moduli that are close to experimental values. The notable exception is the bulk modulus of bcc Cr from

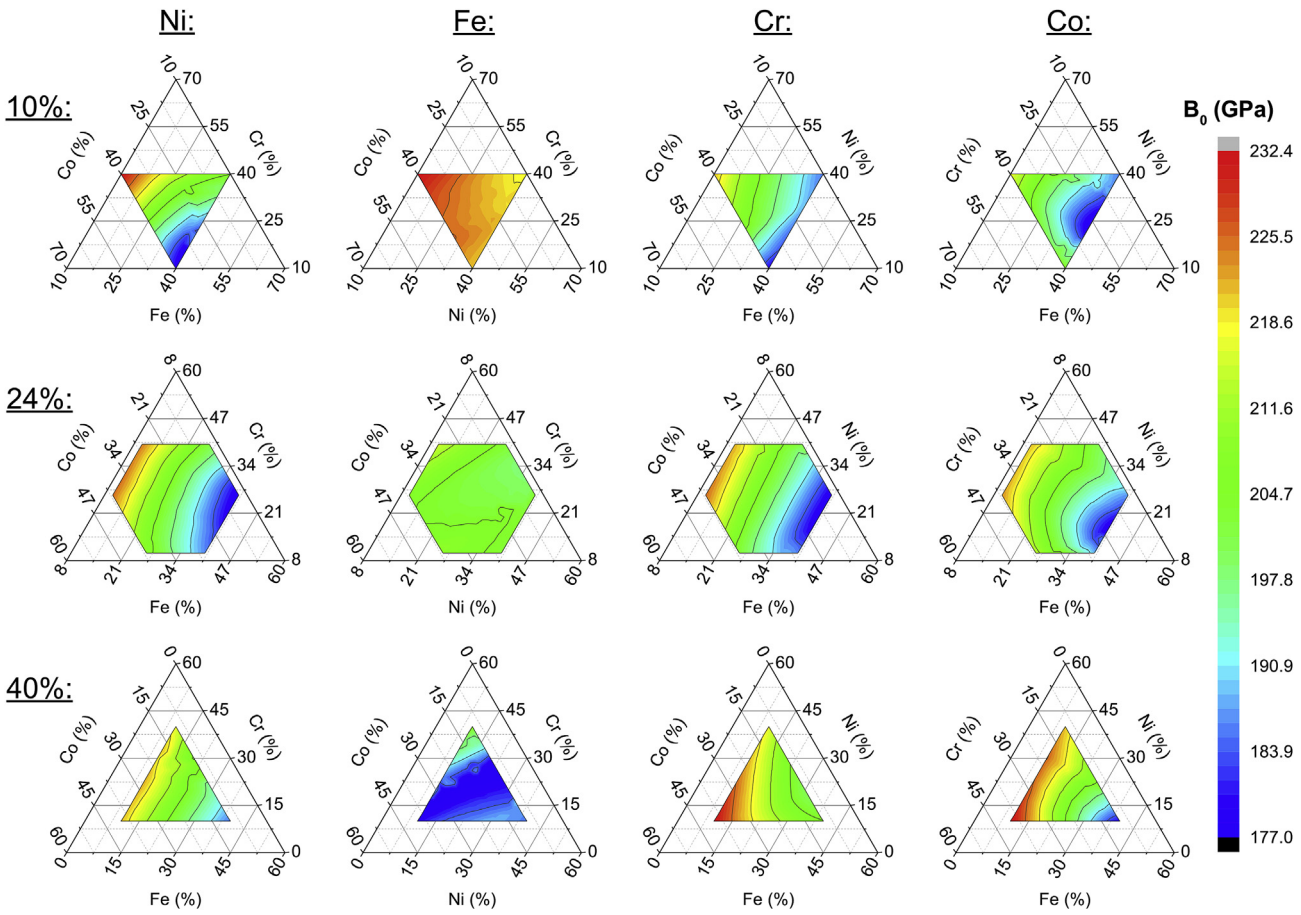

Fig. 4. Bulk modulus, B_0, as a function of composition in Ni–Fe–Cr–Co HEAs.

Table 4
Top 3 alloys with highest/lowest bulk modulus.

Ni,Fe,Cr,Co%	B_0 (GPa)	Ni,Fe,Cr,Co%	B_0 (GPa)
24, 40, 26, 10	177	10, 10, 40, 40	232
10, 40, 16, 34	177	12, 10, 40, 38	231
22, 40, 26, 12	178	12, 10, 38, 40	231

EMTO (256 GPa), which is much larger than the experimental value (190 GPa). We attribute this to the fact that the EMTO-CPA predicts bcc Cr to be non-magnetic while it is an anti-ferromagnetic metal in experiments. VASP predicts bcc Cr to be anti-ferromagnetic with a bulk modulus of 178 GPa, which is in much closer agreement to the experimental value. For the sake of comparison of the two methods, non-magnetic bcc Cr is also simulated by VASP. VASP predicts the NM bcc Cr has a bulk modulus of 260 GPa, showing good agreement with the EMTO method and support for our hypothesis that the large EMTO bulk modulus is due to the predicted magnetic state. While the EMTO approach does not capture the magnetic state of pure bcc Cr, we show in a later section that EMTO does a reasonably good job of capturing the magnetic state and trends in magnetic state as a function of composition as compared to spin polarized VASP calculations.

Table 5
Bulk moduli (GPa) of fcc pure metals and binary alloys from EMTO-CPA.

Metal	B_0	Alloy	B_0	Alloy	B_0
Ni	202	NiFe	173	FeCo	155
Fe	100	NiCr	229	CrCo	251
Cr	232	NiCo	227		
Co	255	FeCr	229		

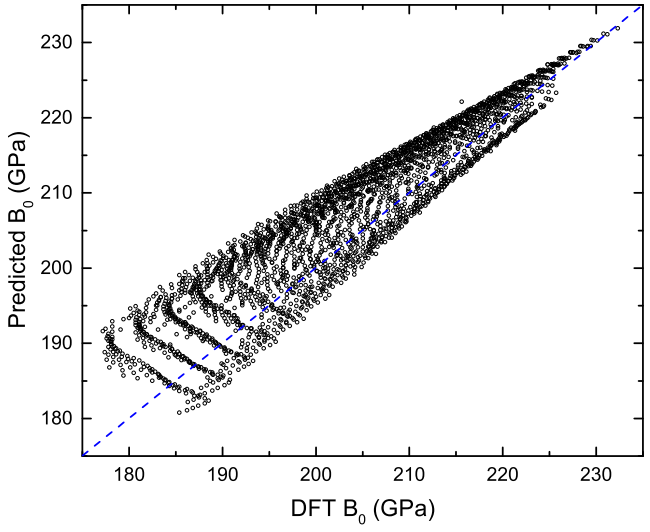

Fig. 5. Bulk modulus from DFT calculations vs. predicted values with binary results. The two values are the same on the blue dashed line (For interpretation of the references to color in this figure legend, the reader is referred to the web version of this article.).

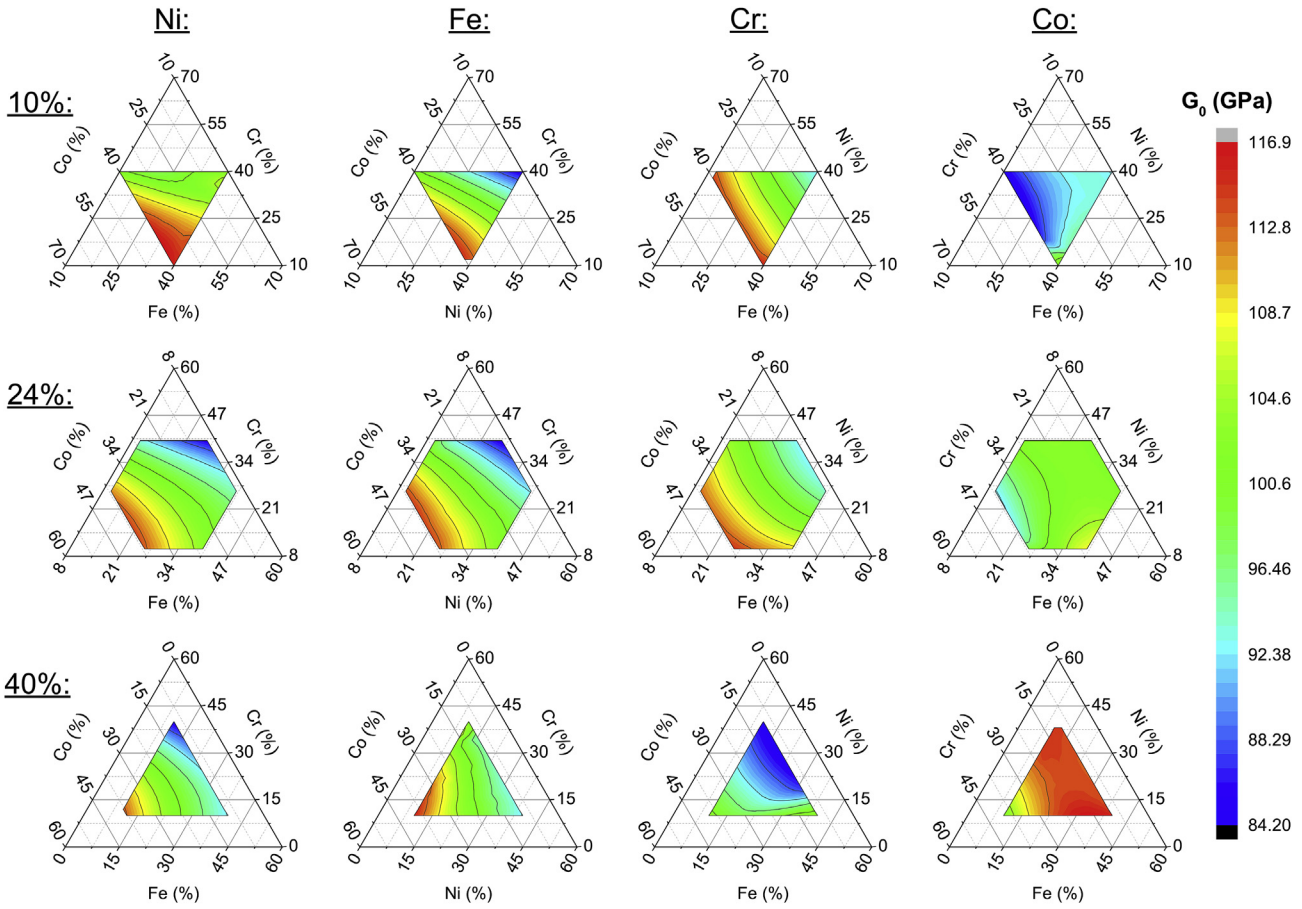

Fig. 6. Shear modulus, G_0, as a function of composition in Ni–Fe–Cr–Co HEAs.

The enthalpy of mixing for 6 fcc binary equiatomic alloys was calculated by the EMTO-CPA method. This included the determination of the bulk energy of each pure element in an fcc reference phase. Because we were interested in predicting the paramagnetic (PM) bulk properties of the quaternary alloys, we determine the energies for the fcc binary alloys and pure metals in the paramagnetic state through implementation of the disordered local moment approximation. Enthalpy of mixing for the 6 fcc binary alloys are given in Table 2. In comparing our EMTO results to those from previous theoretical calculations for binary liquids [48], we find reasonable qualitative agreement between the two sets of data. Specifically, a strongly negative enthalpy of mixing in our fcc solid calculations is also strongly negative for the corresponding binary liquid alloys. Our most positive enthalpies are also the most positive enthalpies in binary liquid mixtures.

3.1.3. *Multi-component enthalpy of mixing from binary data*

We now look to assess the accuracy of Eq. (6) in predicting the multi-component enthalpy of mixing from binary data. To do this, we compare the enthalpy of mixing determined from Eq. (6) that uses the binary data in Table 2 to the enthalpy of mixing explicitly determined through self consistent EMTO + CPA calculations of the 2736 quaternary compositions.

Fig. 2 presents the enthalpies (black points) determined by self-consistent calculations as compared to the values predicted from the binary data through Eq. (6). The blue dashed line is where the values determined from Eq. (6) are exactly the same as those from explicit self-consistent calculations of the alloy. Eq. (6) does a reasonable job of estimating the enthalpy of mixing as all calculated values generally fall near the blue dashed line. We calculated the root-mean-squared deviation (RMSD) for these data points and found it to be 42 meV. This implies that Eq. (6) is expected to be able to predict the enthalpy of mixing for HEAs with an error of 42 meV. While this is a relatively large error, Eq. (6) still provides a reasonable estimate of the trends in enthalpy of mixing from equiatomic binary systems. The advantage of this is binary enthalpy data is more readily available in the literature and is more straightforward from a computational perspective. For accuracy, full self-consistent calculations should be performed.

Table 6
Top 3 alloys with highest/lowest shear modulus.

Ni,Fe,Cr,Co%	G_0 (GPa)	Ni,Fe,Cr,Co%	G_0 (GPa)
34, 16, 40, 10	84	10, 34, 16, 40	117
32, 18, 40, 10	84	10, 36, 14, 40	117
36, 14, 40, 10	84	10, 32, 18, 40	117

3.2. *Lattice parameter*

How the lattice parameter, a_0, of these alloys changes as a function of composition was also explored. Contour plots for a_0 are presented in Fig. 3. Co has the most significant influence on the lattice parameter a_0 of Ni–Fe–Cr–Co HEAs. This is most obvious when comparing the average values found in the three ternary contour maps presented in the Co column. Only slight fluctuations of a_0 are observed within each ternary slice at fixed concentration of Co and there are large changes between one contour map as

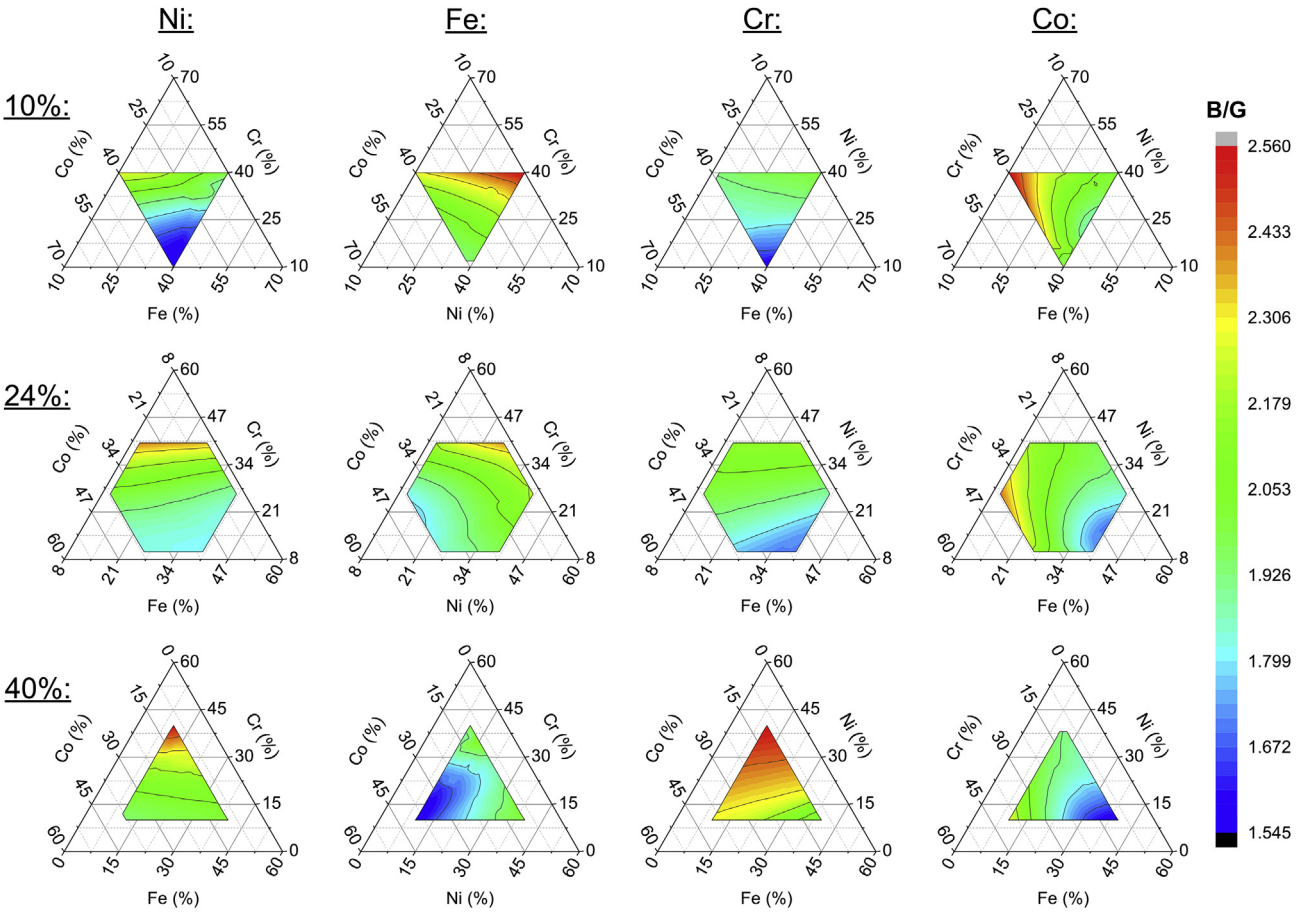

Fig. 7. B/G ratio as a function of composition in Ni–Fe–Cr–Co HEAs.

compared to contour maps in other rows of this column. The significant influence of Co on a_0 is also demonstrated in other slices: red regions in fixed concentrations of Ni-40%, Fe-10% and Cr-40% all locate near the corner where Co is 10%, and dark blue regions in Ni-40%, Fe-10% and Cr-10% all locate where Co is about 40%. The other element that has a large impact on a_0 is Cr: the Cr-10% slice has low/medium a_0, the Cr-24% slice has medium a_0, and the Cr-40% slice has medium/high a_0.

The 12 slices in Fig. 3 demonstrate how each component affects a_0 by using a small portion of all calculated compositions. We also present the top three compositions with either the smallest and largest a_0 among all tested compositions in Table 3. The smallest a_0 is approximately 3.509 Å, found near $Ni_{40}Fe_{10}Cr_{10}Co_{40}$. The largest a_0 is about 3.545 Å, found near $Ni_{40}Fe_{10}Cr_{40}Co_{10}$.

3.3. Bulk modulus

Fig. 4 shows the bulk modulus of Ni–Fe–Cr–Co HEAs. It is found that Fe has a significant influence on bulk modulus of these alloys. 10% Fe leads to highest bulk modulus and 40% Fe leads to lowest. The black solid lines in each sub-plot of Fe/Cr/Co are more or less parallel to grid lines of Fe%, indicating a small correlation of bulk modulus to concentrations of Ni/Cr/Co. The top 3 alloys with the lowest or highest bulk modulus are listed in Table 4. Not surprisingly, the concentration of Fe is 40% in all three alloys with the lowest bulk modulus and 10% in those with the highest bulk modulus.

Bulk modulus describes the resistance of a material against hydrostatic pressure, and can be directly connected to the bonding strength between atoms. We have calculated the bulk moduli of binary random alloys as well as pure metals using the four elements in Table 5. These binary alloys and pure metals are in the fcc lattice with the same magnetic settings as in the NiFeCrCo alloys. Note that fcc Fe has the smallest bulk modulus of all four elements while another significantly low bulk modulus is found in fcc FeCo. This indicates weaker bonding between Fe–Fe and Fe–Co atoms. An alloy with higher Fe concentration, therefore, is expected to have a weaker average bonding strength and a lower bulk modulus. If the bulk modulus is mostly controlled by first-nearest-neighbor chemistry, it should follow the following relation:

$$B_0^{\text{predict}} = \sum_i c_i^2 B_0^i + \sum_{i>j} 2c_i c_j B_0^{ij} \tag{7}$$

where i,j indicate elemental types.

Using Eq. (7), we calculated the predicted bulk moduli of all tested compositions of Ni–Fe–Cr–Co alloys, and found good agreement with the DFT results, as shown in Fig. 5. The RMSD of the Eq. (7) is 6 GPa. Taking into account systematic numerical errors in fitting DFT results to equations of states to determine the bulk modulus, this prediction is rather accurate. Such proportional combination of binary bulk modulus in the forced same lattice structure with the same magnetic settings to predict the bulk modulus of alloys in the near-equiatomic range may be extended to other high-entropy alloys, although preliminary test of selected compositions is suggested to confirm this approach.

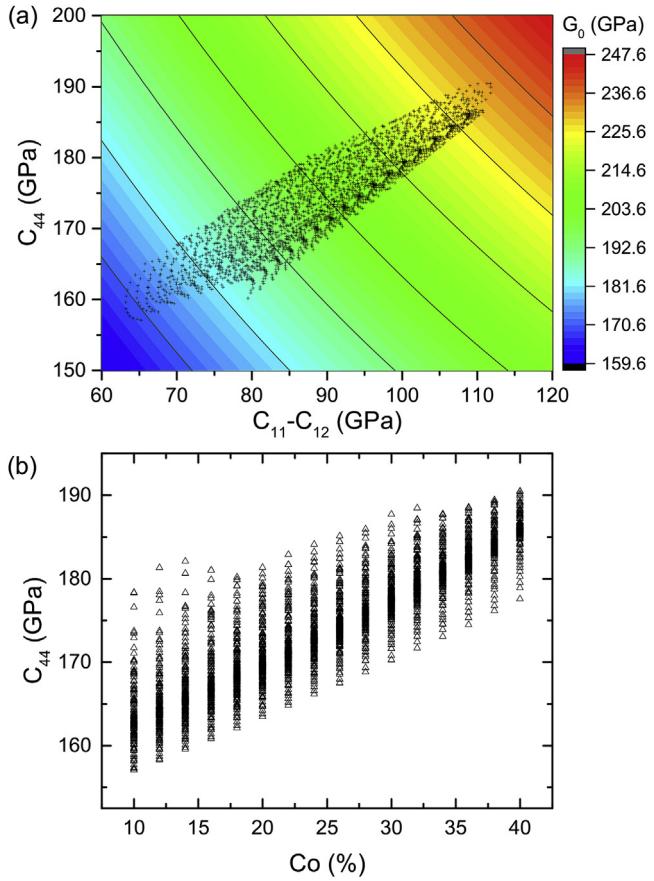

Fig. 8. (a) $C_{11} - C_{12}$ vs. C_{44} for all 2736 alloys in this study plotted on top of shear modulus contour maps. Shear modulus is a function of $C_{11} - C_{12}$ and C_{44}. (b) C_{44} as a function of Co concentration of all alloys.

3.4. Shear modulus

Shear modulus was derived from elastic constants. The elastic constants of a cubic structure that is mechanically stable must satisfy $C_{11} - C_{12} > 0$ and $C_{44} > 0$ [46]. All alloys in the present study were found to fulfill the mechanical stability tests.

Shear modulus G_0 depending on the composition of Ni–Fe–Cr–Co HEAs is plotted in Fig. 6. It is shown that Co slices have fewer color scales and clear gaps between each other, which indicates that Co concentration plays a major role for G_0. Ni–Fe–Cr–Co HEAs with higher concentration of Co have higher shear moduli. The large dark blue region in Cr-40% indicates that high-Cr compositions are more likely to have a low G_0. The large red regions in Ni-10% implies the tendency of low G_0 alloys forming with low Ni concentrations. These trends about Co, Cr and Ni agrees with the top 3 compositions for lower and upper bounds of G_0 in Table 6. All of the three alloys with the lowest G_0 consist of 10% Co and 40% Cr while all those with the highest G_0 have 40% Co and 10% Ni.

Table 7
Comparison of lattice parameters, bulk moduli, and shear moduli from four types of calculations: EMTO-CPA with paramagnetic (PM) settings, EMTO-CPA with spin polarization (SP) settings, VASP with SP settings on unrelaxed lattice, and VASP with SP settings on fully relaxed lattice.

	Ni,Fe,Cr,Co%	$EMTO_{PM}$	$EMTO_{SP}$	$VASP_{SP}$	$VASP_{SP,unrel.}$
a_0	40,10,10,40	3.509	3.539	3.530	3.529
(Å)	40,10,40,10	3.545	3.546	3.552	3.543
B_0	24,40,26,10	177	169	147	161
(GPa)	10,10,40,40	232	215	201	211
G_0	34,16,40,10	84	81	62	74
(GPa)	10,34,16,40	117	82	77	84

3.5. B/G ratio

The ratio of bulk modulus and shear modulus (B/G) is often employed to estimate the ductile/brittle property of materials [51,52]. The Pugh's ratio, or B/G, has been applied to HEAs in the literature [33,53]. When $B/G > 1.75$, the material is more ductile; otherwise it is brittle. This ratio for Ni–Fe–Cr–Co HEAs is mapped in Fig. 7. As shown in the legend of Fig. 7, colors from light blue to red corresponds to $B/G > 1.75$, which covers the majority of all maps. The only dark blue region (most brittle) locates at the low-Ni high-Fe low-Cr high-Co corner, while the red region (most ductile) is at the opposite corner for each component. By comparing the area of these regions, we found Ni–Fe–Cr–Co HEAs are more likely to have brittle characteristics with maximum Fe and minimum Ni and ductile with maximum Cr. However, it must be pointed out that this conclusion is based on the assumption that the alloy stays single phase. It has been mentioned in the section of enthalpy of mixing that high Cr may lead to secondary intermetallic phases, such as the sigma phase. The sigma phase is extremely hard and brittle, whose formation leads to huge changes to mechanical properties [30]. The conclusion derived from those contour maps needs to be carefully evaluated in such cases where it is likely that a secondary phase forms.

It is of interest to determine how the concentration of Co influences the shear modulus of Ni–Fe–Cr–Co HEAs. First, we plotted the shear modulus G_0 as a function of two variables, $C_{11}-C_{12}$ and C_{44}, based on the Voigt-Reuss-Hill averaging equations as a contour map in Fig. 8 (a). We also plotted the $C_{11} - C_{12}$ vs. C_{44} data of all 2736 compositions on top of the contour map. It is found that the $C_{11} - C_{12}$ vs. C_{44} of tested alloys gather as a stripe along the gradient direction of shear modulus. Consequently one can approximate G_0 by considering only C_{44}. In Fig. 8(b), C_{44} was plotted as a function of the concentration of Co. We found a general positive correlation between Co% and C_{44}. Therefore, it is concluded that the Co component contributes to C_{44} in the Ni–Fe–Cr–Co HEAs, which in turn controls shear modulus. This contribution from Co is unlikely to be associated with self-interaction between Co atoms in that C_{44} of fcc Co is quite small (only 160 GPa), but rather originates from the complex chemical bonding with other elements. Unlike bulk modulus that can be conveniently predicted through binary bulk moduli in the same lattice and Eq. (7), shear modulus, on the other hand, is sensitive to C_{44} of the alloy, which is determined by collective local cluster interactions.

3.6. Comparison between EMTO and VASP

We have discussed the enthalpy of mixing, lattice parameters, bulk moduli, and shear moduli of Ni–Fe–Cr–Co HEAs that were obtained through the EMTO-CPA method, which simulated the alloy in the paramagnetic state. We also performed VASP + SQS calculations for selected alloys with the highest or lowest lattice parameter, bulk modulus, or shear modulus found in the paramagnetic state. SQS models were built by considering the first shell correlation functions of pairs within the restriction of the fcc lattice and 100 atoms. Paramagnetic simulation using VASP is non-trivial, so spin polarized (SP) settings were used. SP calculations for the same alloys were also performed by the EMTO-CPA method. Compared to the EMTO-CPA method, which captures perfect chemical disorder but does not include atomic relaxation, the VASP + SQS method allows full atomic relaxation but chemical

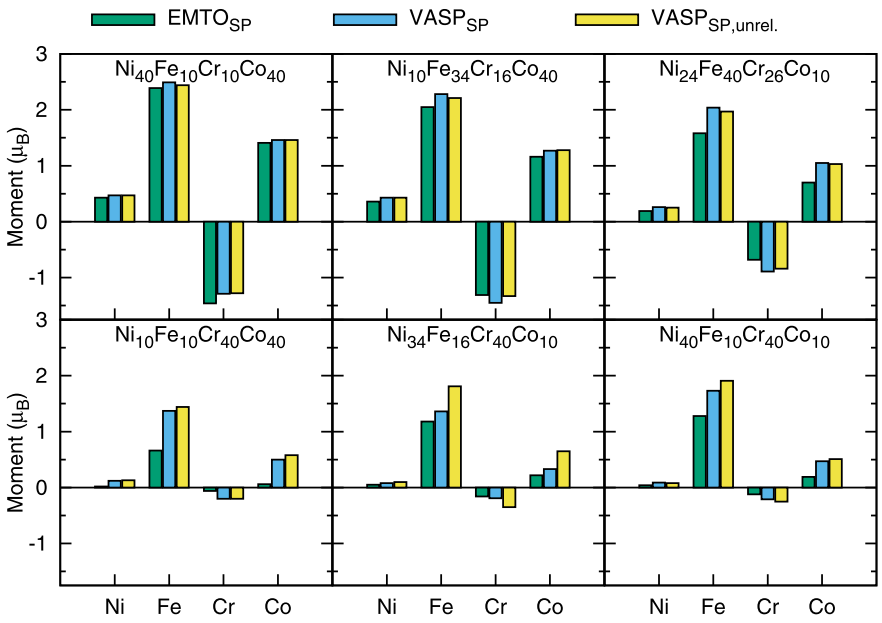

Fig. 9. Average magnetic moment of each element from spin polarized (SP) calculations using EMTO, VASP, and VASP with unrelaxed atoms on the ideal fcc lattice sites of the six alloys as listed in Table 7.

disorder is limited by the randomness captured by the SQS. As such, we have also compared the EMTO-CPA results to VASP-SQS calculations in which no relaxations are performed. This allows for determination of the influence of atomic relaxation in the calculated properties. Table 7 presents the results from EMTO-CPA (paramagnetic and spin polarized (SP)) and VASP + SQS spin polarized calculations with and without atomic relaxations for comparison.

As shown in Table 7, the ETMO-CPA calculations in the PM state generate a_0, B_0 and G_0 results that differ from the spin polarized calculations from either VASP or EMTO-CPA. In comparing only results that include spin polarization, those from EMTO-CPA are generally closer to those from unrelaxed SQS VASP calculations. This is especially the case in comparing elastic properties predicted by both methods and less the case for lattice parameters. Comparing spin polarized calculations to paramagnetic alloys provides perspective on how the magnetic state of the alloy can influence the physical property of interest. For example, Ni_{10} Fe_{34} Cr_{16} Co_{40} has a substantial change in shear modulus as a function of magnetic state while other alloy compositions are more insensitive to this change. While the absolute values predicted for a_0, B_0 and G_0 change as a function of magnetic state, the trends of alloys with high and low values are preserved as a function of composition.

Previously it was noted that pure bcc Cr does not converge to the correct anti-ferromagnetic ground state in the EMTO-CPA approach. This does create an issue in calculating enthalpies of formations straight from the EMTO-CPA approach but it is unclear how it influences the predictions of trends of magnetic moments as a function of alloy composition. It is, therefore, of interest to explore how well the EMTO-CPA approach captures changes in local atomic moments in spin polarized calculations that can be directly compared to complementary VASP SQS calculations. Fig. 9 presents a comparison of average local moments of each elements in the six compositions investigated using the VASP SQS approach. Generally, the magnetic moments from EMTO and VASP agree quite well. This agreement, however, becomes more qualitative as the concentration of Cr increases (bottom row of Fig. 9). Interestingly, unlike the mechanical properties, the magnetic moments from the unrelaxed VASP calculations are not significantly closer to those from EMTO. The agreement of magnetic moments between EMTO and VASP demonstrates that the EMTO calculations can be trustworthy in capturing magnetic trends despite the issues found in bulk Cr.

4. Conclusions

We have systematically studied the high entropy alloy NiFeCrCo in the range of near-equal atomic concentrations, i.e., 10–40 at.%, by first-principles tools and high throughput calculations. Enthalpy of mixing, lattice parameter (a_0), bulk modulus (B), and shear modulus (G) were calculated by the exact muffin-tin orbital method combined with coherent potential approximation (EMTO-CPA) for over 2700 compositions of the NiFeCrCo alloy as a single-phase solid solution in paramagnetic state. These properties were mapped onto contour slices of the composition space. It was found that certain elements have the most significant influence on each property, namely, Cr on enthalpy of mixing, Co on a_0, Fe on B, Co on G, and Cr on the ratio of B/G. An equation to predict the enthalpy of mixing by use of binary enthalpy data was evaluated and was found to have a good accuracy with a root-mean-square deviation (RMSD) of 42 meV per formula unit in the prediction. A similar equation to predict bulk modulus with weighted contribution from first–shell interaction is proposed and tested on all alloys. This equation was also found to be accurate with a RMSD of 6 GPa. Finally, it was found that shear moduli of all tested alloys are largely dependent on C_{44}, while the concentration of Co has a noticeable control on C_{44}. Alloys predicted to have the lowest or highest $a_0/B/G$ in ferromagnetic state were also simulated by EMTO-CPA and the Vienna *ab-initio* Simulation Package (VASP) with special quasi-random structure (SQS) models. Good agreement was found between these methods when similar spin polarization approaches were implemented.

Acknowledgments

CN, AJZ, CCK, and DLI acknowledge support for this work from the National Science Foundation from the Metals and Metallic Nanostructures program under grant DMR-1104930. DLI and CN would also like to acknowledge Levente Vitos for sharing his EMTO-CPA code, version 5.7, for work on this project.

References

[1] J.-W. Yeh, S.-K. Chen, S.-J. Lin, J.-Y. Gan, T.-S. Chin, T.-T. Shun, C.-H. Tsau, S.-Y. Chang, Adv. Eng. Mater 6 (2004) 299–303.
[2] B. Cantor, I. Chang, P. Knight, A. Vincent, Mater. Sci. Eng. A 375–377 (2004) 213–218.
[3] D.B. Miracle, J.D. Miller, O.N. Senkov, C. Woodward, M.D. Uchic, J. Tiley, Entropy 16 (2014) 494–525.
[4] X.F. Wang, Y. Zhang, Y. Qiao, G.L. Chen, Intermetallics 15 (2007) 357–362.
[5] O. Senkov, G. Wilks, J. Scott, D. Miracle, Intermetallics 19 (2011) 698–706.
[6] M. Hemphill, T. Yuan, G. Wang, J. Yeh, C. Tsai, A. Chuang, P. Liaw, Acta Mater 60 (2012) 5723–5734.
[7] M.-H. Chuang, M.-H. Tsai, W.-R. Wang, S.-J. Lin, J.-W. Yeh, Acta Mater 59 (2011) 6308–6317.
[8] X. Yang, Y. Zhang, Mater. Chem. Phys. 132 (2012) 233–238.
[9] K.M. Youssef, A.J. Zaddach, C. Niu, D.L. Irving, C.C. Koch, Mater. Res. Lett. 3 (2014) 95–99.
[10] M. Laurent-Brocq, A. Akhatova, L. Perrière, S. Chebini, X. Sauvage, E. Leroy, Y. Champion, Acta Mater 88 (2015) 355–365.
[11] K.-Y. Tsai, M.-H. Tsai, J.-W. Yeh, Acta Mater 61 (2013) 4887–4897.
[12] F. Otto, Y. Yang, H. Bei, E. George, Acta Mater 61 (2013) 2628–2638.
[13] D. Ma, B. Grabowski, F. Körmann, J. Neugebauer, D. Raabe, Acta Mater 100 (2015) 90–97.
[14] C. Niu, A.J. Zaddach, A.A. Oni, X. Sang, J.W. Hurt III, J.M. LeBeau, C.C. Koch, D.L. Irving, Appl. Phys. Lett. 106 (2015) 161906.
[15] M.S. Lucas, G.B. Wilks, L. Mauger, J.A. Muñoz, O.N. Senkov, E. Michel, J. Horwath, S.L. Semiatin, M.B. Stone, D.L. Abernathy, E. Karapetrova, Appl. Phys. Lett. 100 (2012) 251907.
[16] A. Tamm, A. Aabloo, M. Klintenberg, M. Stocks, A. Caro, Acta Mater 99 (2015) 307–312.
[17] A. Zaddach, R. Scattergood, C. Koch, Mater. Sci. Eng. A 636 (2015) 373–378.
[18] A. Gali, E. George, Intermetallics 39 (2013) 74–78.
[19] B. Gludovatz, A. Hohenwarter, D. Catoor, E.H. Chang, E.P. George, R.O. Ritchie, Science 345 (2014) 1153–1158.
[20] G. Salishchev, M. Tikhonovsky, D. Shaysultanov, N. Stepanov, A. Kuznetsov, I. Kolodiy, A. Tortika, O. Senkov, J. Alloys Compd. 591 (2014) 11–21.
[21] F. Otto, N. Hanold, E. George, Intermetallics 54 (2014) 39–48.
[22] W. Ji, W. Wang, H. Wang, J. Zhang, Y. Wang, F. Zhang, Z. Fu, Intermetallics 56 (2015) 24–27.
[23] C. Zhu, Z. Lu, T. Nieh, Acta Mater 61 (2013) 2993–3001.
[24] A.J. Zaddach, C. Niu, C.C. Koch, D.L. Irving, JOM 65 (2013) 1780–1789.
[25] F. Tian, L.K. Varga, J. Shen, L. Vitos, Comput. Mater. Sci. 111 (2016) 350–358.
[26] F. Körmann, D. Ma, D.D. Belyea, M.S. Lucas, C.W. Miller, B. Grabowski, M.H.F. Sluiter, Appl. Phys. Lett. 107 (2015) 142404.
[27] S. Huang, A. Vida, D. Molnár, K. Kádas, L.K. Varga, E. Holmström, L. Vitos, Appl. Phys. Lett. 107 (2015) 251906.
[28] A. Zaddach, C. Niu, A. Oni, M. Fan, J. LeBeau, D. Irving, C. Koch, Intermetallics 68 (2016) 107–112.
[29] R. Kozak, A. Sologubenko, W. Steurer, Z. für Kristallogr. - Cryst. Mater. 230 (2015) 55–68.
[30] M.-H. Tsai, K.-Y. Tsai, C.-W. Tsai, C. Lee, C.-C. Juan, J.-W. Yeh, Mater. Res. Lett. 1 (2013) 207–212.
[31] L. Vitos, Phys. Rev. B 64 (2001) 014107.
[32] L. Vitos, I. Abrikosov, B. Johansson, Phys. Rev. Lett. 87 (2001) 156401.
[33] F. Tian, L.K. Varga, N. Chen, L. Delczeg, L. Vitos, Phys. Rev. B 87 (2013) 075144.
[34] S. Huang, W. Li, S. Lu, F. Tian, J. Shen, E. Holmström, L. Vitos, Scr. Mater. (2015) 1–4.
[35] G. Kresse, J. Furthmüller, Comput. Mater. Sci. 6 (1996) 15–50.
[36] G. Kresse, Phys. Rev. B 54 (1996) 11169–11186.
[37] P. Blöchl, Phys. Rev. B 50 (1994) 17953–17979.
[38] G. Kresse, Phys. Rev. B 59 (1999) 1758–1775.
[39] A. Zunger, S. Wei, L. Ferreira, J. Bernard, Phys. Rev. Lett. 65 (1990) 353–356.
[40] A. van de Walle, P. Tiwary, M. de Jong, D. Olmsted, M. Asta, A. Dick, D. Shin, Y. Wang, L.-Q. Chen, Z.-K. Liu, Calphad 42 (2013) 13–18.
[41] J.P. Perdew, K. Burke, M. Ernzerhof, Phys. Rev. Lett. 77 (1996) 3865–3868.
[42] J.P. Perdew, K. Burke, M. Ernzerhof, Phys. Rev. Lett. 78 (1997) 1396.
[43] F.J. Pinski, J. Staunton, B.L. Gyorffy, D.D. Johnson, G.M. Stocks, Phys. Rev. Lett. 56 (1986) 2096–2099.
[44] M. Methfessel, A.T. Paxton, Phys. Rev. B 40 (1989) 3616–3621.
[45] M. Hebbache, M. Zemzemi, Phys. Rev. B 70 (2004) 5–10.
[46] M.J. Mehl, B.M. Klein, D.A. Papaconstantopoulos, W. Dc, in: J.H. Westbrook, R.L. Fleischer (Eds.), Intermet. Compd. Princ. Pract. Vol. I Princ., vol. 1, John Wiley and Sons, London, 1995, pp. 195–210.
[47] G. Grimvall, Thermophysical Properties of Materials, Elsevier, 1999.
[48] A. Takeuchi, A. Inoue, Mater. Trans. 46 (2005) 2817–2829.
[49] A. Takeuchi, A. Inoue, Mater. Sci. Eng. A 304–306 (2001) 446–451.
[50] C. Kittel, Introduction to Solid State Physics, eighth ed., John Wiley and Sons, 2005.
[51] S. Pugh, Philos. Mag. 45 (1954) 823–843.
[52] D.G. Pettifor, Mater. Sci. Technol. 8 (1992) 345–349.
[53] F. Tian, L. Delczeg, N. Chen, L.K. Varga, J. Shen, L. Vitos, Phys. Rev. B 88 (2013) 085128.